Enantiotropic ferroelectric nematic phase in a single compound

Jakub Karcz[1], Natan Rychłowicz[1], Małgorzata Czarnecka[2], Antoni Kocot[3], Jakub Herman[1], Przemysław Kula[1]

[1]Institute of Chemistry, Faculty of Advanced Technologies and Chemistry, Military University of Technology, ul. gen. S. Kaliskiego 2, 00-908 Warsaw, Poland
[2]Faculty of Electrical Engineering, Automatics, Computer Science and Biomedical Engineering, AGH University of Science and Technology, al. Adama Mickiewicza 30, 30-059 Cracow, Poland
[3]Institute of Materials Engineering, Faculty of Science and Technology, University of Silesia, ul. 75 Pułku Piechoty, 41-500 Chorzów, Poland

Abstract

The ferroelectric nematic phase became the centre of interest of scientists because of its unique physical properties. The uniqueness of this particular phase results in its monotropic character in all known NF materials. Here we present the very first example of a compound with an enantiotropic ferroelectric nematic phase. Compound 3JK is complementary with already well known NF materials i.e. RM734 and DIO and is characterized by moderately high dielectric anisotropy.

Introduction

Ferroelectric nematic (N_F) materials are a class of liquid crystals that exhibit a unique type of nematic phase with both orientational and translational order[1], [2]. Unlike conventional nematic materials, which have only orientational order, N_F materials have a combination of long-range orientational and translational order, driven by the presence of permanent dipole moments in the molecules. This makes them of great interest for a wide range of applications, including displays, sensors, and nonlinear optics[3], [4]. The discovery of the N_F phase was made independently by Mandle et al.[5] and Nishikawa et al.[6], with subsequent confirmation by Chen et al.[2], and it sparked worldwide scientific interest in the synthesis and physical properties research of this fascinating new class of liquid crystalline materials.
The properties of polar nematic materials are strongly influenced by the nature and structure of the molecules used to form the liquid crystal[7]. The design and synthesis of new molecules with appropriate dipole moments, shapes, and sizes are significant for the development of new polar ferroelectric nematic materials with desirable properties. In recent years, there has been extensive research in the field of ferroelectric nematic materials, with a particular focus on the design, synthesis, and characterization of new materials[8]–[17]. This has led to the discovery of a wide range of N_F materials with novel and interesting properties.
However, the design of ferroelectric nematic materials involves a delicate balance between molecular shape, flexibility, and intermolecular interactions, and requires careful tuning of these factors to achieve the desired phase behaviour[3], [18], [19]. With ongoing advances in the design and synthesis of new materials, it is expected that the properties and performance of polar ferroelectric nematic materials will continue to improve, making them an increasingly important and versatile class of liquid crystals.
Our work focuses on the development of organic materials exhibiting a temperature broad and stable N_F phase, built on aromatic ester derivatives. The material we present, abbreviated as 3JK, is composed of several chemical units of different nature, which, when combined appropriately, form an N_F phase that exists over a wide temperature range and, most

importantly, first example exhibiting an N_F phase with enantiotropic character. The investigated material exhibits common chemical building units that can be categorized into three types: (1) aromatic mesogens with 2,5-substituted 1,3-dioxane groups (DIO analogue[6]); (2) aromatic mesogens with an oriented ester bond (RM734 analogue[5]); (3) aromatic mesogens with an electron-withdrawing fluorocarbon ether group, with additional fluorine atoms laterally substituted in aromatic rings (UUQU-4-N analogue[16]). All these units are arranged sequentially in the same direction to create a controllable magnitude of molecular dipole moment. The structure of the investigated compound is shown in Figure 1.

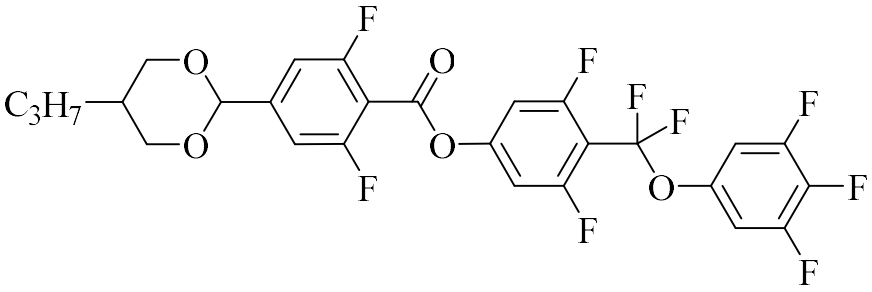

Figure 1. Chemical structure of investigated material 3JK.

Experimental

Materials

1-bromo-3,5-difluorobenzene was purchased from Trimen Chemicals (Łódź, Poland) and used as received. Magnesium for Grignard reactions (turnings), oxalyl chloride were purchased from Acros-Organics, (Geel, Belgium) and used as received. Toluene, acetone, hydrochloric acid were purchased from Avantor Performance Materials Poland S.A (Gliwice, Poland) and used as received. [1,1′-Bis(diphenylphosphino)ferrocene]dichloropalladium(II) was purchased from Sigma-Aldrich Sp. z.o.o (Poznan, Poland) and used as received. Pyridine was purchased from Lach-ner (Neratovice, Czech Republic) and used as received. THF was distilled from sodium under nitrogen atmosphere prior to use.

Synthesis

Synthesis of proposed material is multistep procedure in which various methods were applied – see Figure 2. Benzaldehyde derivative **(2)** was obtained by reacting dimethylformamide with the organomagnesium species produced from 1-bromo-3,5-difluorobenzene **(1)**. Subsequently, an acetal (dioxane) unit was produced **(3)** by reaction with the 2-propylpropane-1,3-diol, and it acts as one of the rings of the liquid crystal core. Carboxylic acid derivative **(4)** was obtained by carboxylation of previously produced lithium derivatives. The last step in the synthesis is the reaction to form an ester bridge between aromatic rings, using the appropriate acid chlorides with a phenol derivative. Earlier, in parallel reactions, the bromo-aromatic reactant was first converted into the corresponding boronic ester **(6)**, which was then transformed into the phenol **(7)** using oxidation procedure. Final liquid crystal material 3JK was successfully isolated and purified using the combination of liquid chromatography and recrystallization techniques.

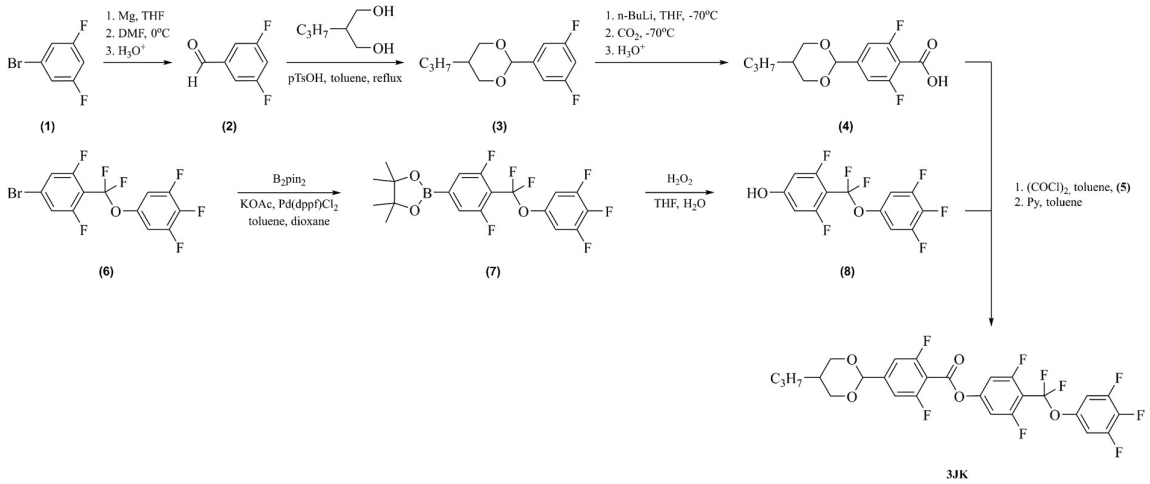

Figure 2. Synthetic route of 3JK.

Synthetic procedures

3,5-difluorobenzaldehyde (2)

Magnesium flakes (12.0g; 0.5mol) and THF (300cm^3) were placed in a 2dm^3 flask and stirred under nitrogen. Small amount of THF solution of 1-bromo-3,5-difluorobenzene **(1)** (96g; 0.5mol) was added to initialize proper reaction. Then, the rest of solution was added dropwise. Temperature was controlled in a way to not exceed a 70°C limit. After addition, the reaction mixture was stirred for 3 hours. Next, dimethylformamide (60cm^3; 0.75mol) was added dropwise to the reaction mixture reaction at 0°C, solution was warmed up to room temperature. The mixture was poured into 1500 cm^3 of water and 100 cm^3 of 10% HCl. Crude product was extracted with pentane. Organic layer was washed three times with water, dried over $MgSO_4$ and solvent was evaporated. Product was purified by distillation under reduced pressure.
Yield 30 g (42%)
bp=84-86°C (50mmHg)
MS(EI) m/z: 142 (M+); 113.

2-(3,5-difluorophenyl)-5-propyl-1,3-dioxane (3)

A solution 3,5-difluorobenzaldehyde **(2)** (30g; 0.21mol), 2-propylpropane-1,3-diol (28g; 0.23mol), p-toluenesulfonic acid (0.3g; 2mmol) in toluene (200cm^3) was refluxed for 4h, while collecting water using Dean-Stark apparatus. After the reaction was completed, mixture was washed three times with water, organic layer was dried over $MgSO_4$ and concentrated. Product was purified by distillation under reduced pressure.
Yield 45.6 g (90%).
bp=84-86°C (0.8mmHg)
MS(EI) m/z: 241 (M+); 223, 141, 129.

2,6-difluoro-4-(5-propyl-1,3-dioxan-2-yl)benzoic acid (4)

2-(3,5-difluorophenyl)-5-propyl-1,3-dioxane **(3)** (45g; 0.186mol) was mixed with anhydrous THF (300cm^3) under nitrogen and cooled to −78°C in an acetone/dry ice bath. Solution of n-butyllithium dissolved in cyclohexane–hexane mixture (0.2mol, 2.5M) was added dropwise,

and temperature was kept below −70°C. The reaction mixture was stirred for 2.5h in −78°C. Then the reaction was flushed with gaseous carbon dioxide (not exceeding the -65°C). After the reaction was completed, it was allowed to reach room temperature. 10% solution of H_2SO_4 was added to the mixture. Then the crude product was filtered off, washed with water and hexane. Product was recrystallized three times from hexane-toluene mixture (1:1 v/v).
Yield 28 g (52%).
mp=126°C
MS(EI) m/z: 285 (M+); 269; 241; 185
^{1}H NMR (500 MHz, $CDCl_3$) δ: 11,61 (s, 1H, COOH); 7,15 (d, J=9,5 Hz, 2H, Ar-H); 5,39 (s, 1H, Ar-CH); 4,25 (dd, J=11,5 Hz, 2H, O-CH_2-CH); 3,54 (t, J=11,5 Hz, 2H, O-CH_2-CH); 2,19-2,09 (m, 2H, (OCH_2)-CH-CH_2); 1,38-1,30 (m, 2H. CH-CH_2-CH_2); 1,12-1,08 (m, 2H, CH_2-CH_2-CH_3), 0,93 (t, J=7,5 Hz, 3H, CH_3)
^{13}C NMR (125 MHz, $CDCl_3$) 166.82, 162.23 (d), 160.17 (d), 145.36 (t), 110.30 (d), 109.43 (t), 98.86, 72.56, 33.88, 30.20, 19.52, 14.18

2-(4-(difluoro(3,4,5-trifluorophenoxy)methyl)-3,5-difluorophenyl)-4,4,5,5-tetramethyl-1,3,2-dioxaborolane (7)
A solution of 5-bromo-2-(difluoro(3,4,5-trifluorophenoxy)methyl)-1,3-difluorobenzene **(6)** (15g ; 0.038mol), bis(pinacolato)diboron (10g ; 0.038mol), anhydrous potassium acetate (11g ; 0.11mol) in toluene (300cm^3) and 1,4-dioxane (300cm^3) was flushed with nitrogen at 80°C for 1h. Then the catalyst Pd(dppf)Cl_2 (3mol%) was added and reaction was stirred at 80°C for 5h. Next reaction was cooled to room temperature and poured into 5% HCl solution. Product was extracted with toluene; organic layer was washed three times with water and dried over $MgSO_4$. Solvent was evaporated under vacuum. Product was recrystallized from ethanol.
Yield 10g (60%),
mp=94°C.
MS(EI)m/z: 437; 421; 289; 207; 189
^{1}H NMR (500 MHz, $CDCl_3$) δ: 7,40 (d, J=10 Hz, 2H, Ar-H), 6,98 (m, 2H, Ar-H); 1,37 (s, 12H, CH_3)
^{13}C NMR (125 MHz, $CDCl_3$) δ: 160.58 (d), 158.52 (d), 151.98 (q), 149.99 (q), 144.69 (m), 139.43 (t), 137.44 (t), 120.24 (t), 118.07 (dd), 111.69 (m), 107.43 (dd), 84.90, 24.80

4-(difluoro(3,4,5-trifluorophenoxy)methyl)-3,5-difluorophenol (8)
Flask containing 2-(4-(difluoro(3,4,5-trifluorophenoxy)methyl)-3,5-difluorophenyl)-4,4,5,5-tetramethyl-1,3,2-dioxaborolane **(7)** (10g; 0.023mol), 30% solution of H_2O_2 (20cm^3), tetrahydrofuran 100cm3 and water 100cm^3 was mixed at 50°C for 4h. After the reaction was completed THF was evaporated and 5% HCl solution was added. Product was extracted with dichloromethane, organic layer was washed three times with water, dried over $MgSO_4$ and concentrated. Product was recrystallized twice from hexane.
Yield 28 g (52%).
mp=190°C
MS(EI) m/z: 326 (M+); 307; 179
^{1}H NMR (500 MHz, $CDCl_3$) δ: 8,19 (s, 1H, OH); 6,96 (m, 2H, Ar-H); 6,47 (d, J=11 Hz, 2H, Ar-H)

^{13}C NMR (125 MHz, $CDCl_3$) δ: 162.05 (d), 160.59 (t), 160.02 (d), 151.95 (q), 149.96 (q), 144.94 (m), 139.30 (t), 120.58 (t), 107.33 (dd), 101.75 (m), 100.42 (dd)

4-(difluoro(3,4,5-trifluorophenoxy)methyl)-3,5-difluorophenyl 2,6-difluoro-4-(5-propyl-1,3-dioxan-2-yl)benzoate (3JK)

In the first stage acid chloride ***2,6-difluoro-4-(5-propyl-1,3-dioxan-2-yl)benzoyl chloride (5)*** was synthesized. In the 250cm^3 round-bottom flask ***2,6-difluoro-4-(5-propyl-1,3-dioxan-2-yl)benzoic acid*** **(4)** (1.2g; 4.2 mmol), oxalyl chloride (0.55cm^3; 6mmol), 50cm^3 toluene and DMF (0.1 cm^3) were added and stirred at RT for 5 hours. Then the excess oxalyl chloride was distilled off. In the second stage, the reaction mixture was cooled to room temperature and ***4-(difluoro(3,4,5-trifluorophenoxy)methyl)-3,5-difluorophenol*** **(8)** (1.5g; 4.6mmol) was added. Then anhydrous pyridine (1cm^3; 8.4mmol) was added dropwise at room temperature. The reaction was stirred at RT for 12 hours. Then the reaction mixture was poured into a HCl (10%) solution. The organic layer was washed three times with water, dried over $MgSO_4$, and concentrated on a rotary evaporator. Crude product was purified by liquid column chromatography (dichloromethane as a mobile phase) and recrystallized from ethyl alcohol, yielding white crystals.

Yield 1.5g (60%).

MS (EI) m/z: 593, 447, 347, 269

^{1}H NMR (500 MHz, $CDCl_3$) δ: 7,21 (d, J=9 Hz, 2H, Ar-H); 7,05-6,97 (m, 4H, Ar-H); 5,42 (s, 1H, Ar-CH); 4,27 (dd, J=11,5 Hz, 2H, O-C$\underline{H_2}$-CH); 3,56 (t, J=11,5 Hz, 2H, O-C$\underline{H_2}$-CH); 2,19-2,12 (m, 2H, (OCH_2)-C$\underline{H}$-CH_2); 1,40-1,33 (m, 2H. CH-C$\underline{H_2}$-CH_2); 1,14-1,10 (m, 2H, CH_2-C$\underline{H_2}$-CH_3), 0,95 (t, J=7,5 Hz, 3H, C$\underline{H_3}$)

^{13}C NMR (125 MHz, $CDCl_3$) δ: 162.07 (d), 161.39 (d), 160.00 (d) , 159.33 (d), 158.32, 153.32 (t), 152.02 (q), 150.02 (q), 146.27 (t), 144.52 (t), 139.51 (t), 137.52 (t), 119.93 (t), 110.42 (dd), 108.63 (t), 108.08 (m), 107.49 (dd), 107.12 (dd), 98.69, 72.59, 33.90, 30.21, 19.53, 14.16

Chemical analysis

Synthesis progress and purity of synthesized compounds were determined using SHIMADZU GCMS-QP2010S (Shimadzu, Kyoto, Japan) series gas chromatograph equipped with quadrupole mass analyser MS(EI), high-performance liquid chromatography HPLC-PDA-MS (APCI-ESI dual source) Shimadzu LCMS 2010 EV (Shimadzu, Kyoto, Japan) equipped with a polychromatic UV–VIS detector (Shimadzu, Kyoto, Japan). and by thin layer chromatography (silica gel on aluminium). Proton (1H) and carbon (13C) nuclear magnetic resonance (NMR) spectra in $CDCl_3$ were collected using a Bruker, model Avance III spectrometer (Bruker, Billerica, MA, USA).

POM observation

Microscopic observations were performed using polarizing optical microscope OLYMPUS BX51(Olympus, Shinjuku, Tokyo, Japan) equipped with a Linkam hot stage THMS-600 (Linkam Scientific Instruments Ltd., Tadworth, United Kingdom) with the sample placed between untreated glass plates.

DSC measurements

DSC measurements were performed using differential scanning calorimeter DSC 204 F1 Phoenix instrument (Netzsch, Selb, Germany) with the scanning rate was 2 $Kmin^{-1}$ on both the heating and cooling cycles with the isothermal time of 5 minutes between cycles.

Dielectric spectroscopy measurements

The complex dielectric permittivity measurements of 3JK sample are measured in planar and homeotropic cells using dielectric analyzers HP- 4192A and HP- 4294. Commercial 5μm cells (WAT-3 Poland) are used, coated with 150- 200 nm gold and of low sheet resistance (R<0.1 Ω/□).

DFT calculations

DFT calculations were performed in Gaussian 16 (Revision C.01)[20] program package with B3LYP[21], [22] functional and 6-311+G(d,p)[23] basis set on the PLGrid ASK Cyfronet Ares cluster.

Results and discussion

To determine the phase behaviour of investigated material, POM observations were performed, followed by DSC measurements. The transition temperatures and associated enthalpies of transitions are given in Table 1. Investigated material 3JK shows enantiotropic ferroelectric nematic as well as conventional nematic phase. Nematic phase was assigned by observation of marble-like texture (Figure 3a). The texture of the N_F phase depends on the measurement cycle. Appearing from the crystal phase, the N_F phase shows a texture of large areas of opposite polarizations with unregular boundaries (Figure 3b), whereas after cooling from the isotropic liquid, the highly birefringent texture with clearly visible boundaries appeared (Figure 3c).

Table 1. Phase behaviour from DSC measurement of 3JK.

	Phase transition temperatures [°C] and enthalpies [$kJmol^{-1}$]
heating cycle	Cr 73.3 [24.29] N_F 87.8 [0.5] N 116.6 [0.57] Iso
cooling cycle	Iso 115.6 [0.57] N 86.8 [0.32] N_F 50.9 [18.79] Cr

Figure 3. POM textures of 3JK. a) Marble-like texture of N phase (T=115°C), b) N_F texture in the heating cycle (T=85°C), c) N_F texture in the cooling cycle (T=85°C).

Phase diagrams of binary mixtures of 3JK with RM734 and DIO were constructed and analysed via POM observations, in both heating and cooling cycles, as shown in Figures 4 and 5. In the mixture with RM734, during the heating cycle, the N_F phase was observed for compositions with an excess of 3JK and in the equimolar mixture, with temperatures of phase transitions close to that of the pure 3JK compound. As the concentration of RM734 increased, the N_F phase

disappeared, and for molar fractions greater than or equal to 0.6, only the conventional nematic phase was observed, again with comparable phase transition temperatures to pure RM734.
On the other hand, in the cooling cycle, both compounds were found to be fully miscible at all concentrations, with a nearly linear change of Iso-N and N-N_F temperatures. As the molar fraction (x) increased, the range of the nematic (N) phase increased throughout the entire phase diagram. The range of the N_F phase initially increased with the increase of x, reaching a peak at x=0.6 (N_F range of 75.5°C), and then decreased afterwards.

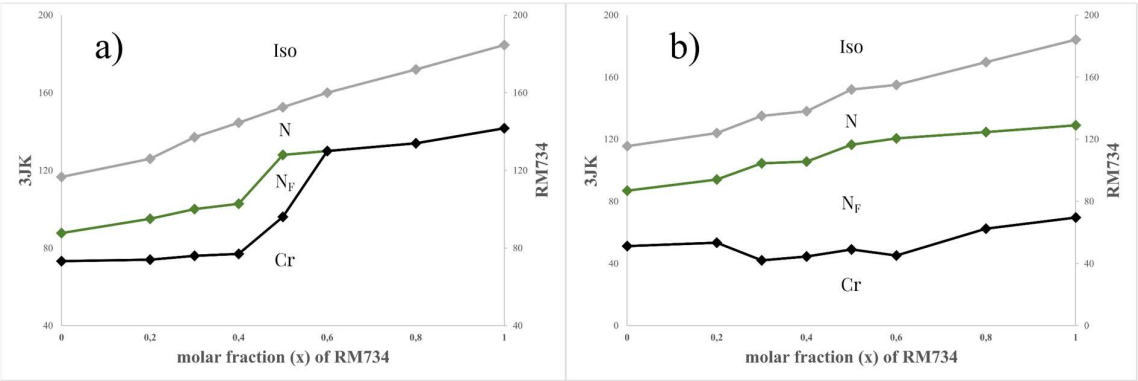

Figure 4. Phase diagrams of binary mixtures of 3JK and RM734 in heating (a) and cooling (b) cycles.

Similar behaviour was observed in mixtures of 3JK with DIO. In the heating cycle the N_F phase was induced in mixtures up to molecular fraction equal to 0.6 with the slight change of N_F-N transition temperatures. In the cooling cycle, as well as previously, the stable N_F phase was observed at all concentrations with the temperature range reaching over 80°C. Additionally, the SmZ_A phase was induced at mixtures with molar fraction greater or equal to 0.2. Overall, 3JK showed better compatibility in mixtures with DIO than with the RM734, due to the higher molecular similarity.

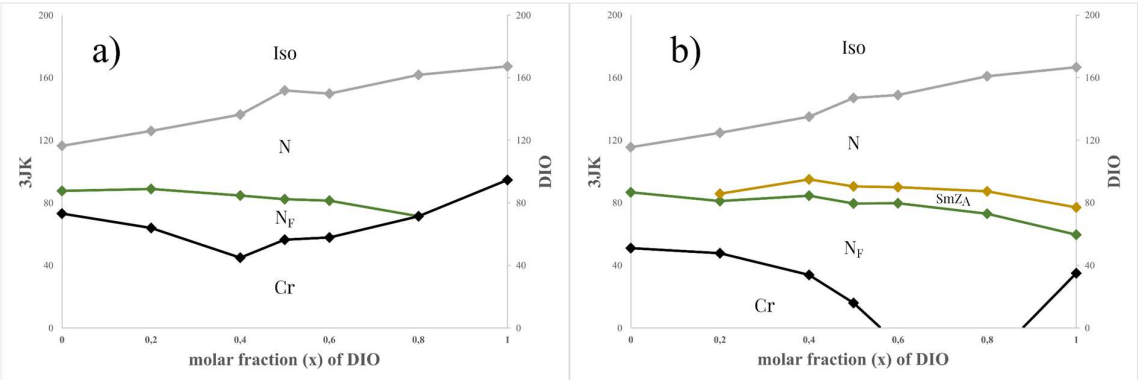

Figure 5. Phase diagrams of binary mixtures of 3JK and DIO in heating (a) and cooling (b) cycles.

The optimized structure of the 3JK was calculated using B3LYP/6-311+G(d,p) level of theory. On this basis, the dipole moment and molecular dimensions were calculated. 3JK is characterized by dipole moment equal 11.96 Debye and molecular dimensions (regarded to atomic van der Vaals volumes): length 27.54 Å, width 8.83 Å, height 6.32 Å. Figure 7 shows the electrostatic potential surface of 3JK. The division of a compound into a surface charge density waves is clearly visible, which aligns well with the model presented by

Madhusudana[24], suggesting that these waves are responsible for parallel orientation of the molecules, hence promoting the polar order and formation of ferroelectric nematic phase.

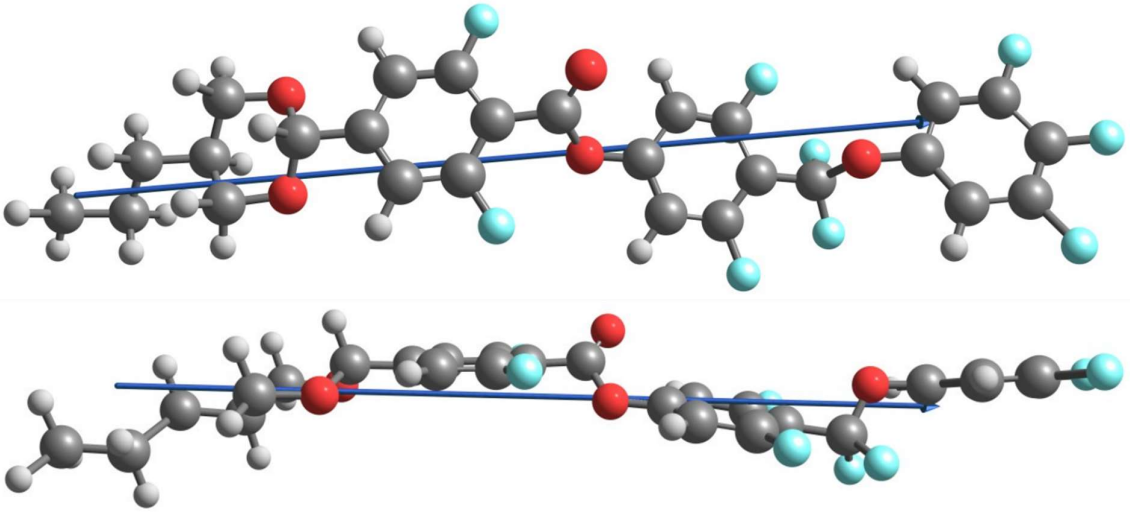

Figure 6. Optimized structure of 3JK.

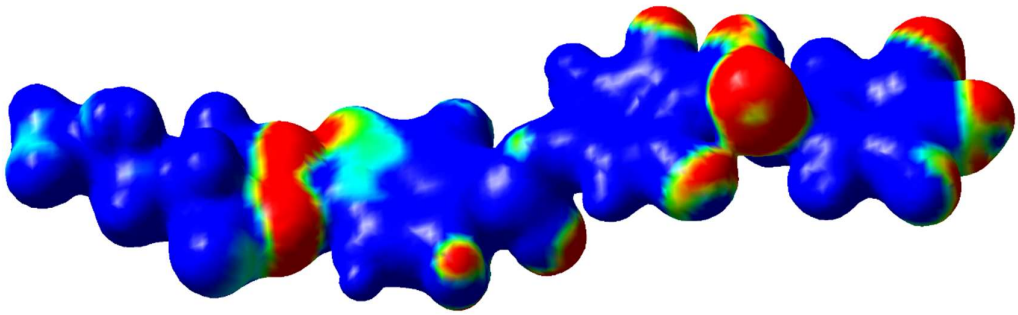

Figure 7. Electrostatic potential surface of 3JK (isovalue 0.04).

Dielectric spectroscopy measurements

The measurements on the aligned liquid crystalline samples were carried out under cooling in the temperature range from 120 °C to 40 °C. The temperature was varied in steps of 1 °C under the application of a weak voltage of 0.02 V. Temperature of the cells with the sample aligned was stabilized to within a range of ±0.02 °C The temperature dependence of the real and imaginary components of the complex permittivity in the frequency range of 5 Hz to 110 MHz were measured in both homeotropic and planarly aligned cells of 5 μm thickness under slow cooling from the isotropic phase. The dielectric measurements indicate the presence of the additional phase (SmZ_A phase) between nematic phases, which was not observed in POM and DSC measurements. The temperature-dependent dielectric loss spectra of longitudinal ($\varepsilon_{\parallel}''$) and transverse ($\varepsilon_{\perp}''$) components of 5 μm thickness cells are shown in Figure 8.

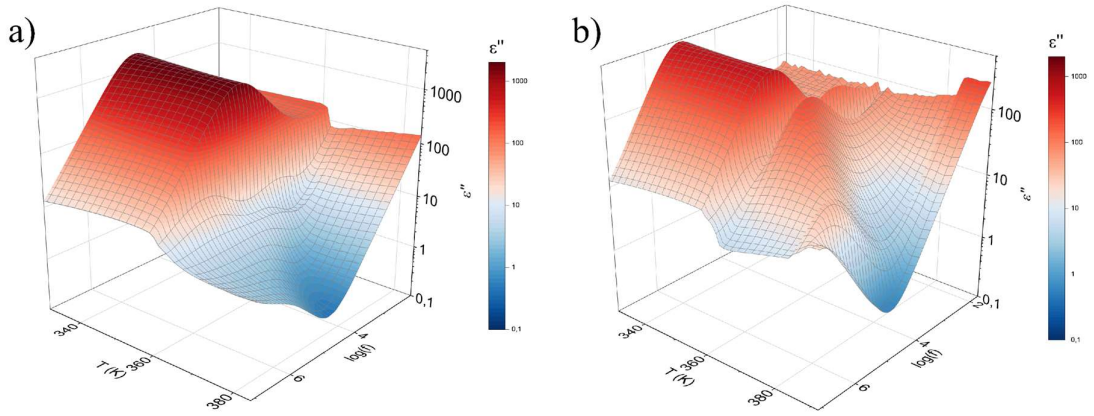

Figure 8. Dielectric loss spectra of a) longitudinal ($\varepsilon_{\parallel}''$) and b) transverse ($\varepsilon_{\perp}''$) components.

The dielectric data on the complex permittivity are fitted to the Cole-Coles equation:

$$\varepsilon*(\omega) = \varepsilon' - i\varepsilon'' = \varepsilon_\infty + \sum \Delta\varepsilon_j / [1+(i\omega\tau_j)^{\alpha}] \qquad (1)$$

where ε_∞ is the high frequency dielectric permittivity depending on the electronic and atomic polarizabilities of the material, $\omega=2\pi f$ is the angular frequency of the probe field, τ_j is the relaxation time of the jth process, $\Delta\varepsilon_j$ is the dielectric amplitude or strength of relaxation process, αj is broadening parameters that determine the distribution of the relaxation times of the jth process.

In the N phase only one relaxation process, **m1**, exist and this is related to the end-over-end rotation of the longitudinal dipole moment, Figure 9. The mode frequency f_1 (~10^6 Hz) and amplitude, $\Delta\varepsilon_1$, well follow the rotational diffusion (RD) model [25], [26] for reorientation of the individual molecules:

$$\frac{f_1}{f_D} = \left(\frac{e^{\sigma}-1}{\sigma}\right)^{-1}\left(\frac{e^{\sigma}-1}{\sigma}\frac{2\sigma\sqrt{\delta/\pi}}{1+\sigma} + 2^{-\sigma}\right) \qquad (2)$$

$$\Delta\varepsilon_1 = \frac{Ag\,\mu_l^{\,2}}{T}(1+2S) \qquad (3)$$

where: f_D is relaxation rate for rotational diffusion in the isotropic phase, σ is nematic potential barrier parameter, approximate expressions for the relaxation times is derived as $\sigma = \frac{3}{2}S(5-\pi S)/(1-S^2)$, μ_l is the longitudinal dipole moment, $A = N'hF^2/3\varepsilon_0 k_B$ is the scaling factor for the relaxation mechanisms that contribute to the complex permittivity, N' is the number density of molecules, ε_0 is the permittivity of vacuum, T is the absolute temperature, k_B is the Boltzmann constant. F and h are the internal field factors for the reaction and cavity fields, respectively. The long-range dipole-dipole interaction can be described by an anisotropic Kirkwood coefficient, g, which is a measure how the dielectric strength increases with respect to the system of uncorrelated dipoles. These coefficients are most accessibly defined as the corresponding dipole correlation functions G(r).

$$g = 1 + V^{-1}\int G(r)dr \qquad G(r) = \frac{\langle\mu(0)\bullet\mu(r)\rangle}{\langle\mu(0)\bullet\mu(0)\rangle} \qquad (4)$$

At the I-N transition frequency mode **m1** drops and amplitude increases ~(1+2S) with increased orientational order S, as predicted by the RD model. At the lower temperature range of the N phase, however, the cooperativity of the molecular rotation becomes apparent. As a result, the frequency decreases and amplitude increases faster(more) than expected following the RD model. The factor, g, grows from unity at high temperatures up to 4 on approaching the low range of the N phase. On transition to the SmZ_A phase, further frequency decrease is observed due to stronger cooperativity. The amplitude of the mode, **m1**, critically decreases (4 times) as the antiferroelectric order of the SmZ_A phase is built up, thus Kirkwood coefficient

returns to unity. Another, high-frequency mode, **m2**, appears in the SmZ_A phase and that shows similar temperature behaviour. The mode **m2** is assigned as azimuthal fluctuation mode, which can be related to the precession mode in the N phase. In the SmZ_A phase, the mode indicates grow of the ferroelectric cooperativity/ferroelectric domains. On approaching the N_F phase both modes show critical behaviour. The amplitude and frequency of the low-frequency mode, **m1**, show soft mode-like behaviour. The amplitude of the high-frequency mode, **m2**, approaches $\Delta\varepsilon$ ~4000, as the ferroelectric order builds up.

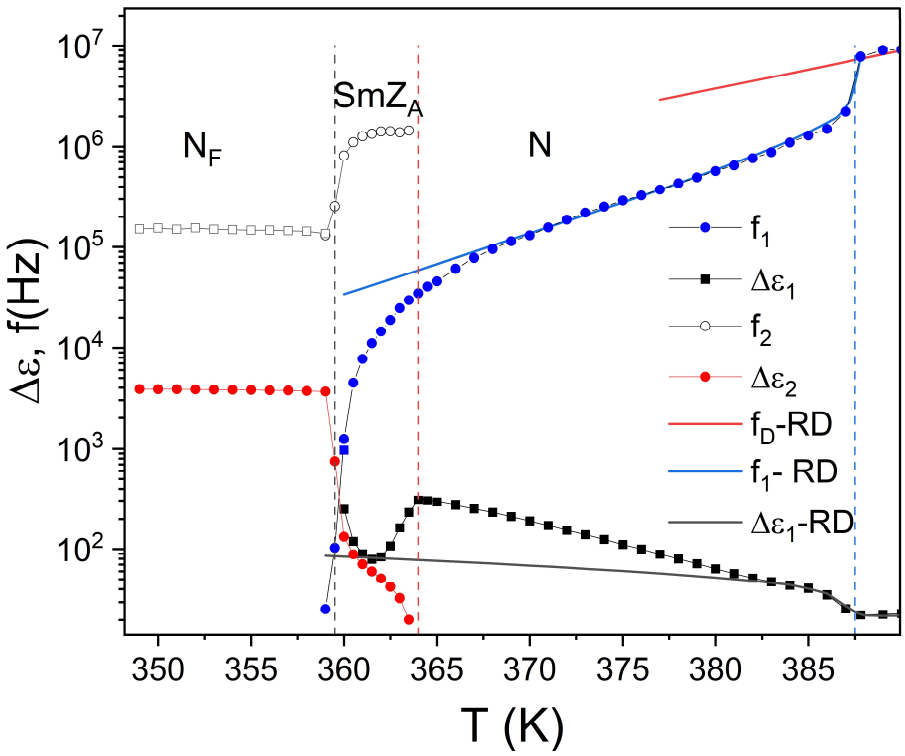

Figure 9. Dielectric properties of the 3JK sample measured in a 5µm-thick cells with gold electrodes with and without aligning polymer layers. Solid lines are predictions of the RD model.

Conclusion

We have successfully designed and synthesized a compound demonstrating the existence of a ferroelectric nematic phase. Through a strategic combination of building blocks found in known N_F materials, we achieved the stabilization of a ferroelectric nematic phase, characterized notably by its enantiotropic nature. This marks the pioneering instance of a ferroelectric nematic material exhibiting such phase behaviour. This type of behaviour is a new discovery, as all N_F materials discovered so far are monotropic ones. In our believe, it opens a new chapter in searching and designing materials selected typically for this particular nematic phase. Compound 3JK exhibits remarkable compatibility with both RM734 and DIO, displaying complete miscibility of their respective nematic phases. Additionally, it induces the enantiotropic N_F phase in binary mixtures. Binary mixture with DIO gives enantiotropic N_F with stable phase down to 0°C. While microscopic observations and calorimetric measurements confirm the presence of nematic phases exclusively, dielectric spectroscopy measurements hint

at the potential existence of the SmZ_A phase. Further exploration and investigation into this phenomenon are underway

Acknowledgements

This work was financed/co-financed by Military University of Technology under research project UGB 22-801. J.K., A.K. and M.C. thank the National Science Centre for funding through grant no. 2022/45/B/ST5/04093. We gratefully acknowledge Poland's high-performance Infrastructure PLGrid (HPC Centers: ACK Cyfronet AGH, PCSS, CI TASK, WCSS) for providing computer facilities and support within computational grant no. PLG/2022/015802.

References

[1] O. D. Lavrentovich, 'Ferroelectric nematic liquid crystal, a century in waiting', *Proc Natl Acad Sci U S A*, vol. 117, no. 26, pp. 14629–14631, Jun. 2020, doi: 10.1073/PNAS.2008947117/ASSET/5EBD6E13-049D-4DBF-BC09-0A7EEA2444BE/ASSETS/GRAPHIC/PNAS.2008947117FIG01.JPEG.

[2] X. Chen *et al.*, 'First-principles experimental demonstration of ferroelectricity in a thermotropic nematic liquid crystal: Polar domains and striking electro-optics contributed new reagents/analytic tools; X', *PNAS*, vol. 117, no. 25, pp. 14021–14031, 2002, doi: 10.17605/osf.

[3] J. Li *et al.*, 'Development of ferroelectric nematic fluids with giant-dielectricity and nonlinear optical properties', *Sci Adv*, vol. 7, no. 17, pp. 5047–5068, Apr. 2021, doi: 10.1126/SCIADV.ABF5047/SUPPL_FILE/ABF5047_SM.PDF.

[4] C. L. Folcia, J. Ortega, R. Vidal, T. Sierra, and J. Etxebarria, 'The ferroelectric nematic phase: an optimum liquid crystal candidate for nonlinear optics', *https://doi.org/10.1080/02678292.2022.2056927*, vol. 49, no. 6, pp. 899–906, 2022, doi: 10.1080/02678292.2022.2056927.

[5] R. J. Mandle, S. J. Cowling, and J. W. Goodby, 'Rational Design of Rod-Like Liquid Crystals Exhibiting Two Nematic Phases', *Chemistry – A European Journal*, vol. 23, no. 58, pp. 14554–14562, Oct. 2017, doi: 10.1002/CHEM.201702742.

[6] H. Nishikawa *et al.*, 'A Fluid Liquid-Crystal Material with Highly Polar Order', *Advanced Materials*, vol. 29, no. 43, p. 1702354, Nov. 2017, doi: 10.1002/ADMA.201702354.

[7] R. J. Mandle, 'A new order of liquids: polar order in nematic liquid crystals', *Soft Matter*, vol. 18, no. 27, pp. 5014–5020, Jul. 2022, doi: 10.1039/D2SM00543C.

[8] R. Saha *et al.*, 'Multiple ferroelectric nematic phases of a highly polar liquid crystal compound', *https://doi.org/10.1080/02678292.2022.2069297*, vol. 49, no. 13, pp. 1784–1796, 2022, doi: 10.1080/02678292.2022.2069297.

[9] E. Cruickshank, A. Pearson, S. Brown, J. M. D. Storey, C. T. Imrie, and R. Walker, 'The ferroelectric nematic phase: on the role of lateral alkyloxy chains', *https://doi.org/10.1080/02678292.2023.2221651*, 2023, doi: 10.1080/02678292.2023.2221651.

[10] E. Cruickshank, R. Walker, J. M. D. Storey, and C. T. Imrie, 'The effect of a lateral alkyloxy chain on the ferroelectric nematic phase', *RSC Adv*, vol. 12, no. 45, pp. 29482–29490, Oct. 2022, doi: 10.1039/D2RA05628C.

[11] N. Tufaha, E. Cruickshank, D. Pociecha, E. Gorecka, J. M. D. Storey, and C. T. Imrie, 'Molecular Shape, Electronic Factors, and the Ferroelectric Nematic Phase: Investigating the Impact of Structural Modifications', *Chemistry – A European Journal*, vol. 29, no. 28, p. e202300073, May 2023, doi: 10.1002/CHEM.202300073.
[12] S. Brown *et al.*, 'Multiple Polar and Non-polar Nematic Phases', *ChemPhysChem*, vol. 22, no. 24, pp. 2506–2510, Dec. 2021, doi: 10.1002/CPHC.202100644.
[13] Y. Song *et al.*, 'Development of emergent ferroelectric nematic liquid crystals with highly fluorinated and rigid mesogens', *Physical Chemistry Chemical Physics*, vol. 24, no. 19, pp. 11536–11543, May 2022, doi: 10.1039/D2CP01110G.
[14] M. Cigl, N. Podoliak, T. Landovský, D. Repček, P. Kužel, and V. Novotná, 'Giant permittivity in dimethylamino-terminated ferroelectric nematogens', *J Mol Liq*, vol. 385, p. 122360, Sep. 2023, doi: 10.1016/J.MOLLIQ.2023.122360.
[15] H. Matsukizono, K. Iwamatsu, S. Endo, Y. Okumura, S. Anan, and H. Kikuchi, 'Synthesis of liquid crystals bearing 1,3-dioxane structures and characterization of their ferroelectricity in the nematic phase', *J Mater Chem C Mater*, vol. 11, no. 18, pp. 6183–6190, May 2023, doi: 10.1039/D2TC05363B.
[16] A. Manabe, M. Bremer, and M. Kraska, 'Ferroelectric nematic phase at and below room temperature', *https://doi.org/10.1080/02678292.2021.1921867*, vol. 48, no. 8, pp. 1079–1086, 2021, doi: 10.1080/02678292.2021.1921867.
[17] R. J. Mandle, 'Supramolecular ferroelectric nematic materials', *https://doi.org/10.1080/02678292.2022.2145380*, vol. 49, no. 15, pp. 2019–2026, 2022, doi: 10.1080/02678292.2022.2145380.
[18] R. J. Mandle, S. J. Cowling, and J. W. Goodby, 'Structural variants of RM734 in the design of splay nematic materials', *Liq Cryst*, vol. 48, no. 12, pp. 1780–1790, 2021, doi: 10.1080/02678292.2021.1934740/SUPPL_FILE/TLCT_A_1934740_SM9249.DOCX.
[19] J. Li *et al.*, 'General phase-structure relationship in polar rod-shaped liquid crystals: Importance of shape anisotropy and dipolar strength', *Giant*, vol. 11, p. 100109, Aug. 2022, doi: 10.1016/J.GIANT.2022.100109.
[20] M. J. Frisch *et al.*, 'Gaussian 16, Revision C.01'. 2016.
[21] C. Lee, W. Yang, and R. G. Parr, 'Development of the Colle-Salvetti correlation-energy formula into a functional of the electron density', *Phys Rev B*, vol. 37, no. 2, p. 785, Jan. 1988, doi: 10.1103/PhysRevB.37.785.
[22] A. D. Becke, 'Density-functional thermochemistry. III. The role of exact exchange', *J Chem Phys*, vol. 98, no. 7, pp. 5648–5652, Apr. 1993, doi: 10.1063/1.464913.
[23] W. J. Hehre, K. Ditchfield, and J. A. Pople, 'Self—Consistent Molecular Orbital Methods. XII. Further Extensions of Gaussian—Type Basis Sets for Use in Molecular Orbital Studies of Organic Molecules', *J Chem Phys*, vol. 56, no. 5, pp. 2257–2261, Mar. 1972, doi: 10.1063/1.1677527.
[24] N. V. Madhusudana, 'Simple molecular model for ferroelectric nematic liquid crystals exhibited by small rodlike mesogens', *Phys Rev E*, vol. 104, no. 1, p. 014704, Jul. 2021, doi: 10.1103/PHYSREVE.104.014704/FIGURES/13/MEDIUM.
[25] P. L. Nordio, G. Rigatti, and U. Segre, 'Dielectric relaxation theory in nematic liquids', *http://dx.doi.org/10.1080/00268977300100141*, vol. 25, no. 1, pp. 129–136, 2006, doi: 10.1080/00268977300100141.
[26] W. T. Coffey and Y. P. Kalmykov, 'Rotational Diffusion and Dielectric Relaxation in Nematic Liquid Crystals', pp. 487–551, Mar. 2007, doi: 10.1002/9780470141724.CH10.